NANO LETTERS

2007
Vol. 7, No. 4
932−940

Toward Control of the Metal–Organic Interfacial Electronic Structure in Molecular Electronics: A First-Principles Study on Self-Assembled Monolayers of π-Conjugated Molecules on Noble Metals

Georg Heimel,*,† Lorenz Romaner,†,‡ Egbert Zojer,†,‡ and Jean-Luc Brédas†

School of Chemistry and Biochemistry and Center for Organic Photonics and Electronics, Georgia Institute of Technology, Atlanta, Georgia 30332-0400, Institute of Solid State Physics, Graz University of Technology, Petersgasse 16, A-8010 Graz, Austria

Received December 11, 2006; Revised Manuscript Received February 8, 2007

ABSTRACT

Self-assembled monolayers (SAMs) of organic molecules provide an important tool to tune the work function of electrodes in plastic electronics and significantly improve device performance. Also, the energetic alignment of the frontier molecular orbitals in the SAM with the Fermi energy of a metal electrode dominates charge transport in single-molecule devices. On the basis of first-principles calculations on SAMs of π-conjugated molecules on noble metals, we provide a detailed description of the mechanisms that give rise to and intrinsically link these interfacial phenomena at the atomic level. The docking chemistry on the metal side of the SAM determines the level alignment, while chemical modifications on the far side provide an additional, independent handle to modify the substrate work function; both aspects can be tuned over several eV. The comprehensive picture established in this work provides valuable guidelines for controlling charge-carrier injection in organic electronics and current–voltage characteristics in single-molecule devices.

Introduction. In recent years, self-assembled monolayers (SAMs) of organic molecules grown on a variety of substrates have been the focus of intense multidisciplinary research.[1−6] Many of these efforts have been directed toward modifying macroscopic surface properties such as wetting or corrosion resistance[7,8] and a variety of applications has been explored including, e.g., nanolithography or chemical sensing.[9−15] In organic (opto)electronic devices, where the importance of the interface energetics at the electrode−organic contact is well acknowledged,[16,17] SAMs have been employed to modify the effective work function (Φ) of the electrodes;[18−26] the latter is directly linked to the barrier for charge carrier injection/extraction into/from the active organic layer.[16,17]

The self-assembly of π-conjugated molecules on noble metal electrode structures has also been central to the emerging field of single-molecule electronics.[27−33] In analogy to the line-up of the electrode Fermi energy with the conducting states in the active organic layer in (macroscopic) organic electronics, the energetic alignment of the metal Fermi level (E_F) with the frontier molecular orbitals (MOs) of the active molecular entity (i.e., the SAM or, alternatively, individual molecules) is a key parameter.[34,35] In such systems, the local chemical, electronic, and geometric structure at the metal−molecule interface is known to have a major impact on the overall device characteristics.[36−38] Given the rather elusive and often fluctuating local geometric structure in single-molecule transport experiments,[39−45] SAMs have been studied on extended, well-defined metal surfaces in order to gain a fundamental understanding of the (dominant) interface energetics in single-molecule devices.[46,47]

Here, we seek to provide general insight into the interface energetics of SAM-covered metals: we investigate separately the impact of each component of a metal−SAM system (Figure 1a): (a) The effect of the headgroup (pointing away from the surface) is briefly revisited.[48] (b) The influence of the π-conjugated core is elucidated by varying its length and thus its electronic structure in a well-controlled manner. (c) While thiols are the most studied docking groups that

* Corresponding author. E-mail: georg.heimel@chemistry.gatech.edu.
† Georgia Institute of Technology.
‡ Graz University of Technology.

10.1021/nl0629106 CCC: $37.00
Published on Web 02/28/2007

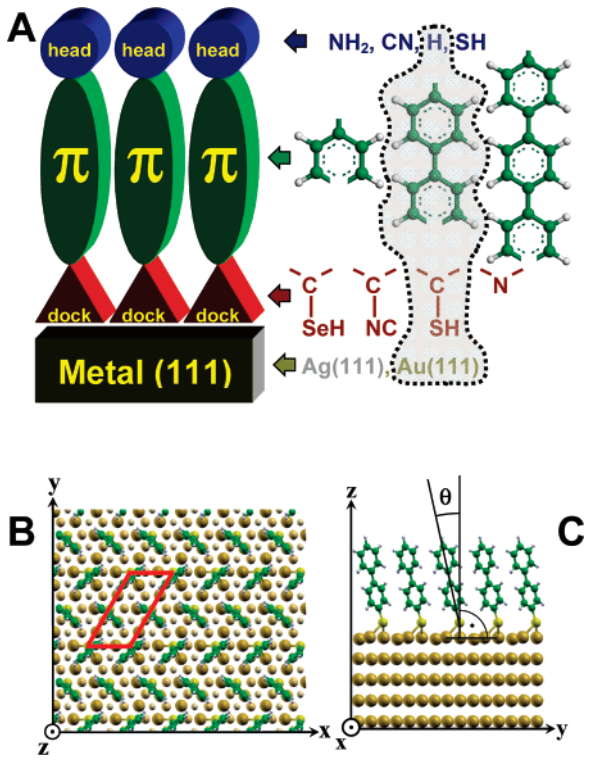

Figure 1. (a) Schematic representation and chemical structure of the systems investigated in this work: SAMs of molecules consisting of a docking group (dock), a π-conjugated core (π), and a headgroup (head) are assembled on Au and Ag(111) surfaces. The encircled structure serves as a reference system. (b) Top view of the SAM structure; the contour indicates the p($\sqrt{3} \times 2\sqrt{3}$)-*R*30° surface unit cell. (c) Side view of the SAM structure; the long molecular axes are tilted from the surface normal by the angle θ.

covalently link organic molecules to coinage metal surfaces, the impact of different docking groups on the interfacial electronic structure is assessed as well.[38,42,45,49−59] (d) The differences between the two most studied substrate metals for SAMs (Au and Ag) are also discussed. By examining the relative importance and interplay of each of these aspects by means of first-principles calculations, we derive a comprehensive microscopic picture and shed light on the underlying mechanisms that determine the interface energetics in plastic and single-molecule electronics. Our findings are also discussed in the broader framework of Schottky barrier formation at junctions between metals and inorganic[60−62] as well as organic[63,64] semiconductors.

Details on the density-functional theory (DFT) calculations employed in the present study are reported in the Supporting Information. The methodology has been extensively tested and benchmarked elsewhere.[65]

The molecules investigated in the present study are shown in Figure 1a. The structure encircled by the dotted contour, 4-mercaptobiphenyl on Au(111), serves as the reference system. Starting from this compound, various headgroups (−SH, −CN, $-NH_2$) are placed on the 4′-position. For the simple hydrogen headgroup (−H) and the Au(111) surface, the length of the conjugated core is varied from one to three rings (1P, 2P, and 3P); in all three cases, the docking groups are varied: thiol (−SH), selenol (−SeH), isocyanide (−NC), and the case where the phenyl ring closest to the metal is replaced by a pyridine. To capture the impact of the substrate metal, the reference molecule (4-mercaptobiphenyl) is studied on the (111) surfaces of both gold and silver. The molecular arrangement within the SAM is shown in Figure 1b and c (see also Supporting Information).

Hereafter, the systems are labeled by listing the components indicated in Figure 1a in the following way: *docking-group*|*number-of-rings*|*headgroup*, when discussing 2D layers of the molecules alone (e.g., SH|2P|H for the reference system, 4-mercaptobiphenyl); and *metal*|*docking-group*|*number-of-rings*|*headgroup*, when discussing SAMs on a metal subtrate [e.g., Au|S|2P|H for the reference system, 4-mercaptobiphenyl on Au(111)]. As indicated by this notation, the −SH and −SeH docking groups are assumed to lose their hydrogen atom upon bonding to the metal. Note that, for the sake of comparability, the *number-of-rings* (1P, 2P, or 3P) indicates the total number of rings in the molecule, phenylene or pyridine.

Results and Discussion. The modification of the effective work function of a metal substrate upon SAM formation has been found to originate from two effects:[16−21,25] (i) the dipole of the molecules, and (ii) an interfacial dipole that incorporates both the effect of the *push-back* of the metal electrons (reduction of the intrinsic surface dipole)[66−70] and the effect of the charge redistribution due to bond formation between the docking group and the metal surface.[16]

Molecular Layers. To evaluate the contribution of (i), the first step is to find, from the orientation θ of the molecules on the surface (Figure 1c), the projection $\mu_\perp$ of the molecular dipole moments μ onto the surface normal via $\mu_\perp = |\boldsymbol{\mu}|\cdot\cos\theta$. With the knowledge of $\mu_\perp$ and the packing density of the molecules in the SAM, one could in principle compute the nominal potential jump, $\Delta\tilde{V}_{vac}$, across the dipolar layer of molecules (no metal surface present) via the Helmholtz equation:[18−21,25]

$$\Delta\tilde{V}_{vac} = -\frac{\mu_\perp}{\epsilon_0 \cdot A} \qquad (1)$$

where A is the size of the surface unit cell (Figure 1b) and ϵ_0 is the vacuum permittivity (see Supporting Information for an extended discussion and the values of μ, $\mu_\perp$, θ, and $\Delta\tilde{V}_{vac}$). This approach, however, does not take into account the fact that the electrostatic interaction between the (dipolar) polarizable molecules leads to a reduction in the dipole moment per molecule in the SAM. Extracting the actual step in the macroscopic electrostatic potential across a single, 2D molecular layer (no metal present) from our self-consistent DFT calculations yields a much smaller ΔV_{vac} (Table 1). While more elaborate models can be found in the literature,[71,72] this mutual *depolarization* of the molecules has frequently been accounted for by simply introducing an additional effective dielectric constant, ϵ_{eff}, into the denominator of eq 1.[18−21,25] Comparing the values for $\Delta\tilde{V}_{vac}$ calculated via eq 1 with those for ΔV_{vac} extracted from the DFT calculations on the 2D molecular layers yields the ϵ_{eff} values listed in Table 1. It is important to note that ϵ_{eff} is

Table 1. Potential Step Across the (Saturated) 2D Infinite Layer of Molecules, ΔV_{vac}, in V; Effective Dielectric Constant of the Molecular Layer, ϵ_{eff}; Left and Right Side Ionization Potential, IP_{left} and IP_{right}, and Electron Affinity, EA_{left} and EA_{right}, in eV[a]

system	ΔV_{vac}	ϵ_{eff}	IP_{left}	IP_{right}	EA_{left}	EA_{right}
SH|1P|H	−0.52	1.91	5.57	5.05	1.49	0.97
SH|2P|H	−0.37[b]	2.22	5.27	4.89	2.18	1.80
SH|3P|H	−0.35	2.41	5.13	4.78	2.48	2.13
SeH|1P|H	−0.52	1.99	5.42	4.90	1.51	0.99
SeH|2P|H	−0.41	2.25	5.24	4.83	2.21	1.80
SeH|3P|H	−0.39	2.48	5.14	4.75	2.52	2.13
CN|1P|H	−3.34	1.96	8.84	5.51	4.80	1.46
CN|2P|H	−3.40	2.26	8.47	5.07	5.38	1.98
CN|3P|H	−3.40	2.46	8.27	4.87	5.60	2.20
Pyr|1P|H	−2.34	1.63	7.09	4.75	3.45	1.11
Pyr|2P|H	−2.45	1.92	7.19	4.74	4.31	1.86
Pyr|3P|H	−2.52	2.30	7.18	4.66	4.65	2.13
SH|2P|CN	3.84	2.30[a]	5.17	9.01	2.34	6.18
SH|2P|NH_2	−1.49	3.09[a]	5.12	3.62	2.19	0.69
SH|2P|SH	0.19[c]		5.08	5.27	2.20	2.39

[a] See text for details on the highlighted numbers. [b] The values for SH|2P|H on Ag (−0.38) is slightly larger than on Au because of the somewhat smaller lattice constant of Ag and thus tighter packing of the molecules in the SAM. [c] For the symmetric substitution, ΔV_{vac} arises from the fact that the (slightly asymmetric) atomic positions of the final relaxed structure of the adsorbed SAM were used for the (hydrogen-terminated) molecular layer.

not simply the static dielectric constant of the π-conjugated core of the molecules, but rather a convenient construct to capture the effect described above. This becomes apparent, e.g., from the fact that for the same core, biphenyl, the value for ϵ_{eff} changes from 2.3 to 3.1[65] in going from SH|2P|CN to SH|2P|NH_2 and thus depends on the headgroup substitution. To explore the connection between the terminal groups and the molecular dipole moment as well as ϵ_{eff}, we analyze the electrostatic potential distribution in these infinite 2D-periodic molecular layers.

In Figure 2a, the electrostatic potential of the molecular layers, as averaged in the *xy* plane (Figure 1), is shown for SH|2P|*x* with *x* = H, SH, CN, and NH_2, together with the energy levels corresponding to the highest occupied and lowest unoccupied MOs (HOMO and LUMO). We emphasize that the situation in the 2D molecular layer is conceptually different from that of a single molecule. In the latter case, a single, well-defined vacuum level permits the unique definition of a single ionization potential (IP) and electron affinity (EA). In the former case, ΔV_{vac} divides space into two regions with different values for the macroscopic electrostatic potential in the vacuum, V_{vac}^{left} on the docking-group side and V_{vac}^{right} on the headgroup side; therefore, there exist two ionization potentials, IP_{left} and IP_{right}, as well as two electron affinities, EA_{left} and EA_{right}.[48,65] The most striking feature in Figure 2a is that the values for IP_{left} and EA_{left} are nearly the same for all four systems, while IP_{right} and EA_{right} depend significantly on the headgroup substitution (Table 1).[48] This implies that the headgroups affect only *their* end of the molecule. The potential distributions in Figure 2a show that, for the molecules investigated here, the dipole moment, and thus ΔV_{vac}, does not arise from long-range intramolecular charge transfer (i.e., isolated charges on either end of the molecule). Rather, they originate from different bond polarizations localized around the headgroups; the potential distributions in the region of the molecular core are virtually identical for all molecules. Moreover, the dependence of ΔV_{vac} on the molecular length is found to be weak (Table 1). The above observation rationalizes also why the choice of the headgroup has a stronger impact on ϵ_{eff} than the length of the π-conjugated core (Table 1).

When keeping the same headgroup (−H) but varying the docking groups, the electrostatic potentials exhibit the opposite behavior (Figure 2b). In this instance, the IP_{right} and EA_{right} values are practically identical, while the IP_{left} and EA_{left} values are markedly different (Table 1); note that the potentials for the −SH and −SeH docking groups lie virtually on top of each other. Thus, the docking groups are also seen to significantly affect only *their* end of the molecular layer; the differences in IP_{left} and EA_{left} values can be attributed to variations in local electrostatic potential due to different bond polarization in the spatial region around the docking groups.

Work-Function Modification. To determine the SAM-induced modification in work function, $\Delta\Phi$, the impact of the bond formation between the isolated layer of molecules and the metal surface needs to be assessed next. The charge rearrangement, ρ_{diff}, occurring at the metal−molecule interface upon bond formation between the molecules and the metal can be extracted from the calculations on the −SH and −SeH docking groups as:[48,65]

$$\rho_{diff} = \rho - (\rho_{Au} + \rho_{Mol} - \rho_{H}) \quad (2.a)$$

where one covalent bond (S−H or Se−H) is *replaced* by another covalent bond (S−Au and Se−Au). For −NC and −Pyr, a new covalent bond is *formed* between molecule and metal, and the expression reads:

$$\rho_{diff} = \rho - (\rho_{Au} + \rho_{Mol}) \quad (2.b)$$

Here, ρ is the total charge density from the self-consistent calculation on the full metal−SAM system, ρ_{Au} is the charge density of the clean metal surface, ρ_{Mol} is the charge density of the molecular layer, and ρ_{H} is the charge density associated with the single layer of hydrogen atoms that needs to be removed upon adsorption of the molecular layers with −SH and −SeH docking groups (see Supporting Information).

In the upper panels of Figure 3, ρ_{diff} is shown for all docking groups and chain lengths on Au(111) with −H as headgroup; results for the −SH and −SeH docking groups once again coincide. The corresponding graphs for Au|S|2P|*x* with *x* = SH, CN, and NH_2 have been reported elsewhere.[48] Analysis of ρ_{diff} leads to the following conclusions: (i) the charge rearrangement is mainly localized around the immediate molecule−metal interface region (with the exception of the pyridine docking group); (ii) no significant net long-range charge transfer between SAM and metal is observed for any system (see Supporting Information).

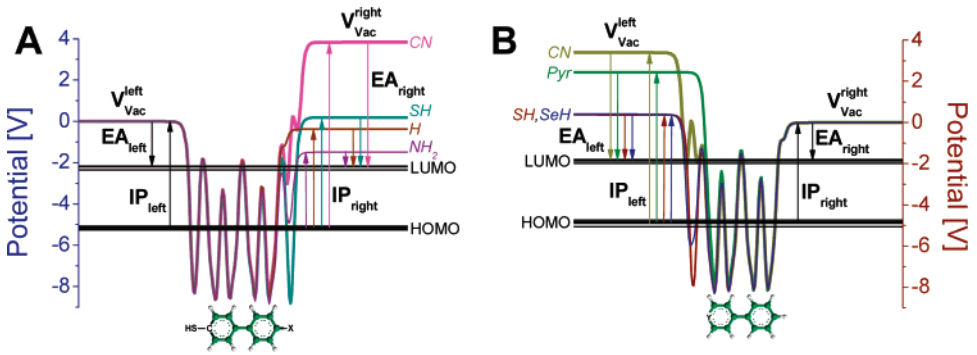

Figure 2. Plane-averaged electrostatic potentials of the isolated 2D molecular layers of: (a) biphenyls with a −SH docking group and −CN (magenta), −SH (cyan), −H (brown), and $-NH_2$ (purple) headgroups; (b) molecules with two π-conjugated rings with a −H headgroup and −NC (yellow), −Pyr (green), −SH (red), and −SeH (blue) docking groups. The horizontal lines indicate the energetic positions of the highest occupied molecular orbitals (HOMO) and lowest unoccupied molecular orbital (LUMO). Also indicated are the left and right vacuum levels (V^{left}_{vac} and V^{right}_{vac}), left and right ionization potentials (IP_{left} and IP_{right}), as well as left and right electron affinities (EA_{left} and EA_{right}).

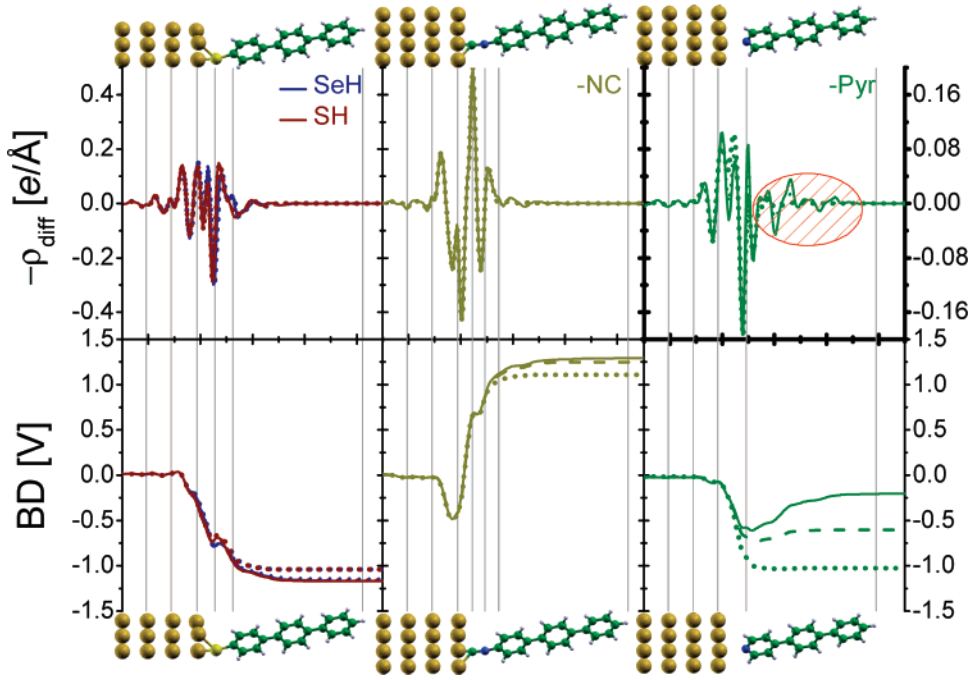

Figure 3. Charge density redistribution ρ_{diff} (top) and resulting bond dipole BD (bottom) that occur upon bond formation between the Au(111) surface and the 2D layers of molecules with one (dotted line), two (dashed line), and three (solid line) π-conjugated rings. All molecules have a −H headgroup. The vertical lines indicate the positions of the gold layers, the docking group atom(s), the first atom in the ring, and the −H headgroup of the longest molecule. Note that the scale of the ordinate in the upper right panel is different from those of the top left and center panels; see text for details on the shaded region in the top right panel.

Importantly, by integrating the one-dimensional Poisson equation, $\nabla^2 V = -\rho_{diff}/\epsilon_0$, the magnitude (Table 2) and spatial extent (Figure 3) of the electrostatic potential step caused by ρ_{diff} can be evaluated; conceptually, this procedure is equivalent to summing over a series of small, localized dipoles by repeatedly applying eq 1. Very much like ρ_{diff}, this potential step is localized around the immediate bonding region between molecule and metal for the −SH, −SeH, and −NC docking groups (Figure 3); hereafter, it will be referred to as the *bond dipole*, BD (we stress that BD incorporates both the reduction of the intrinsic surface dipole of the metal *and* the local charge redistribution due to bond formation). The data in Figure 3 shows that, for the −SH, −SeH, and −NC docking groups, BD exhibits no pronounced dependence on the length of the π-conjugated core of the molecules; it is only in the −Pyr case (where ρ_{diff} extends well into the molecular layer for any length) that a pronounced chain-length dependence is observed. Note that BD can point either way: depending on the choice in docking group, the electrostatic potential immediately outside the interfacial region around the metal−molecule bond is either pulled up (−NC) or pushed down (−SH, −SeH, −Pyr).

With the contributions from both the molecular dipoles and the interfacial bond dipoles in place, $\Delta\Phi$ can now be

Table 2. Bond Dipole, BD, in V; Work Function Modification, $\Delta\Phi$, in eV; Ionization Potential and Electron Affinity of the SAM, IP_{SAM} and EA_{SAM}, in eV; Correction for the Energetic Positions of the Frontier Molecular Orbitals in the SAM, E_{corr}^{HOMO} and E_{corr}^{LUMO}, in eV; and Energetic Position of the Frontier Molecular $\pi[\pi^*]$ States with Respect to the Fermi Level, ΔE_{HOPS} [ΔE_{LUPS}], in eV

system	BD	$\Delta\Phi$	IP_{SAM}	EA_{SAM}	E_{corr}^{HOMO}	E_{corr}^{LUMO}	ΔE_{HOPS}	ΔE_{LUPS}
Au|S|1P|H	−1.05	−1.57	4.72	1.08	0.32	−0.11	−1.09	2.55
Au|S|2P|H	−1.17	−1.55	4.69	1.70	0.21	0.11	−1.03	1.96
Au|S|3P|H	−1.19	−1.54	4.65	2.08	0.13	0.05	−0.98	1.59
Au|Se|1P|H	−1.05	−1.57	4.61	1.04	0.29	−0.05	−0.96	2.61
Au|Se|2P|H	−1.15	−1.57	4.58	1.71	0.25	0.10	−0.93	1.94
Au|Se|3P|H	−1.18	−1.57	4.55	2.07	0.19	0.05	−0.91	1.57
Au|CN|1P|H	1.15	−2.18	5.34	2.43	0.17	−0.97	−2.28	0.63
Au|CN|2P|H	1.28	−2.12	5.06	2.50	0.00	−0.53	−1.94	0.62
Au|CN|3P|H	1.32	−2.09	4.91	2.52	−0.03	−0.32	−1.75	0.64
Au|Pyr|1P|H	−1.01	−3.35	5.65	1.19	−0.90	−0.08	−3.79	0.67
Au|Pyr|2P|H	−0.58	−3.03	5.56	1.97	−0.83	−0.11	−3.37	0.22
Au|Pyr|3P|H	−0.18	−2.71	5.14	2.30	−0.49	−0.18	−2.63	0.21
Au|S|2P|CN	−1.18[a]	2.65[a]	8.84	6.12	0.16	0.05	−0.99	1.73
Au|S|2P|NH_2	−1.20[a]	−2.69[a]	3.47	0.59	0.15	0.10	−0.96	1.92
Au|S|2P|SH	−1.21[a]	−1.02[a]	5.13	2.27	0.13	0.11	−0.95	1.91
Ag|S|2P|H	−0.39	−0.77	4.88	1.76	0.01	0.04	−1.16	1.96

[a] These values deviate slightly (by max 0.02 eV) from those reported in ref 48 because the accuracy of the computational procedure has since been improved. The conclusions drawn in either work are not affected by these minor numerical differences.

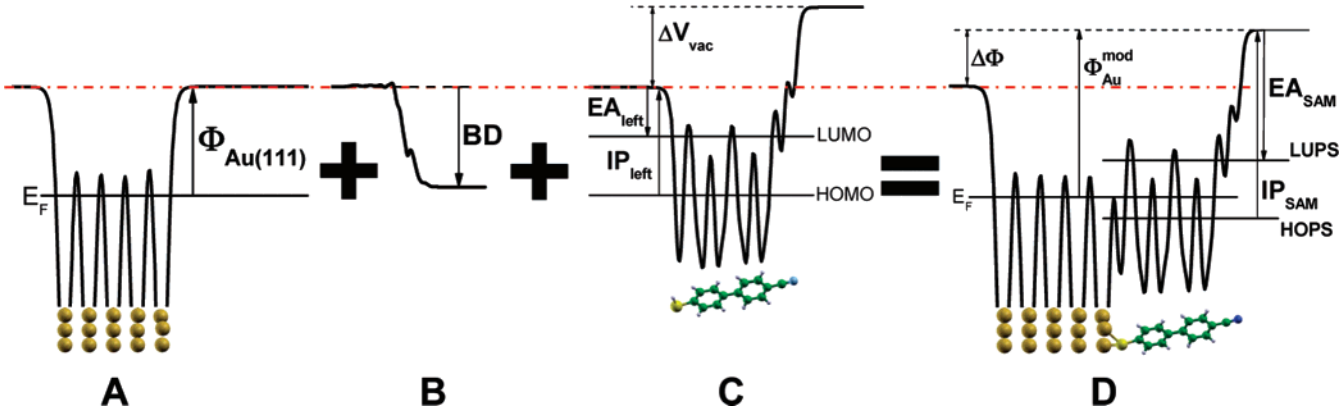

Figure 4. Schematic representation of the changes in electrostatic potential upon SAM formation for the Au|S|2P|CN system: The work function, $\Phi_{Au(111)}$, of the clean gold surface (a) is defined by the difference between its Fermi level, E_F, and the vacuum level (horizontal dash−dotted red line). Upon bond formation, the potential step (b), BD, shifts the potential of the molecular layer (c), down in energy with respect to E_F, leading to the final situation (d). In (c), the left ionization potential and electron affinity, IP_{left} and EA_{left}, are shown. BD realigns these levels with respect to the metal leading to their energetic position in the metal−SAM system (d) with respect to E_F, ΔE_{HOPS}, and ΔE_{LUPS}, and the vacuum level outside the SAM covered surface, IP_{SAM} and EA_{SAM}. The potential step across the dipolar molecular layer, ΔV_{vac} (c), together with BD (b), modifies $\Phi_{Au(111)}$ by $\Delta\Phi$ to yield the work function of the SAM-covered surface, Φ_{Au}^{mod} (d). Note that, for the sake of clarity, the energy scale (*y*-axis) is expanded in (b).

described on the basis of the microscopic picture developed above. The evolution of the interface energetics upon SAM formation is schematically shown in Figure 4 for the Au|S|2P|CN system taken as an example. The two relevant isolated subsystems are the clean metal surface (Figure 4a) with work function $\Phi_{Au(111)}$ and the saturated molecular layer (Figure 4c) with an associated potential step ΔV_{vac} due to the aligned dipole moments of the individual molecules. Upon bond formation between the molecular layer and the clean Au(111) surface, a BD is established (Figure 4b) that pushes the electrostatic potential in the spatial region of the SAM down in energy. This then leads to the final electrostatic potential of the combined metal−SAM system (Figure 4d). The initial work function $\Phi_{Au(111)}$ is modified by $\Delta\Phi$, the sum of ΔV_{vac} and BD, to yield a metal surface with a modified work function, Φ_{Au}^{mod}:[18−21,25]

$$\Delta\Phi = \Delta V_{vac} + BD \tag{3}$$

The calculated values for $\Delta\Phi$ are listed in Table 2. Note that the $\Delta\Phi$s and BDs can also be extracted directly from the self-consistent DFT calculations on the full metal−SAM system; they coincide with those obtained by the procedure outlined above. With −H as a headgroup, all molecules lower

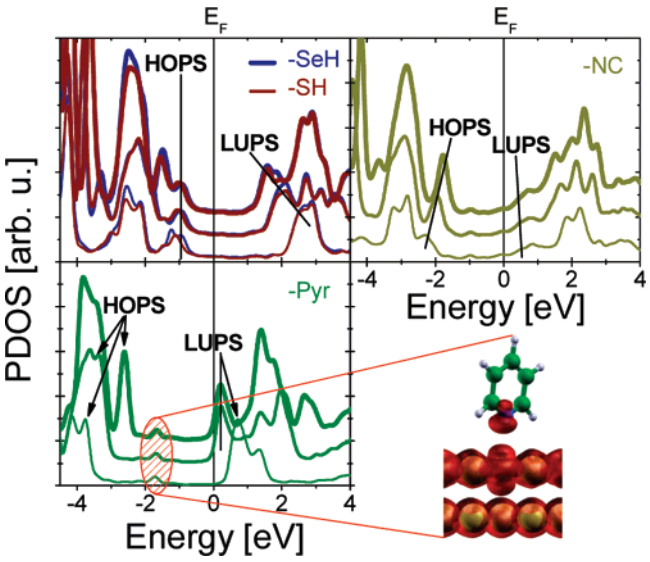

Figure 5. Density of states projected onto the molecular region (PDOS) of the SAM−metal systems for molecules on Au(111) with one (thin line), two (intermediate line), and three (thick line) π-conjugated rings and different docking groups; the headgroup is −H. The graphs have been offset vertically for the sake of clarity. The frontier π- and π*-states are indicated in each case, and the Au−N state is shown in the inset.

the metal Φ upon SAM formation, with the magnitude of the decrease strongly depending on the docking group. Even in the case of the −NC docking group, the strongly positive BD is overcompensated by the molecular dipole ($\Delta V_{vac} \ll 0$), leading to an overall negative $\Delta\Phi$. An increase in Φ is observed only for the −CN headgroup (together with an −SH docking group). This implies that BD together with the built-in dipole of the specific docking group is at least equally important for the SAM-induced modification of the substrate work function as the headgroup;[48] *both the docking group and the headgroup are thus seen to provide largely independent pathways for tuning* Φ. While for the other docking groups, $\Delta\Phi$ is only slightly affected by the conjugation length of the molecules, a marked dependence of $\Delta\Phi$ on molecular length is observed in the case of the −Pyr linker (arising from the strong chain-length dependence of BD for the −Pyr systems). Note that the calculated values for $\Delta\Phi$ are likely to represent an upper limit for what can be observed experimentally because the high coverage and order assumed in the calculations is difficult to achieve in practice, especially for the highly dipolar molecules among those investigated here.[73]

Level Alignment. The density of states of the total metal−SAM system projected onto the molecular region (PDOS)[65] is shown for all docking groups and chain lengths on Au(111) in Figure 5; again, the −SH and −SeH docking groups are seen to behave identically. At this point, it is important to note that it is not straightforward to unambiguously associate the peaks in the PDOS around E_F with any particular MO of the isolated molecule (see Supporting Information). Thus, it appears more adequate to refer to the highest energy peak in the occupied region (below E_F) of the molecular PDOS as *highest occupied* π*-states* (HOPS) and to the lowest energy peak in the unoccupied region (above E_F) as *lowest unoccupied* π*-states* (LUPS) rather than as HOMO and LUMO, respectively.

We find that the frontier molecular π- and π*-states (HOPS and LUPS) come to lie highest with respect to E_F for the −SH (−SeH) docking groups, at intermediate positions for −NC, and lowest for −Pyr; *the choice of the docking chemistry thus permits tuning the level alignment over a range of several eV*. These results are consistent with recent experimental data available for −SH and −NC.[54,59] As discussed elsewhere,[48] the effect of headgroup substitutions on the alignment of the frontier π- and π*-states relative to E_F is negligible (Table 2). In this context, it is important to note that, with the exception of the −Pyr docking group (see inset in Figure 5), no sharp features appear in the PDOS near E_F that could pinpoint the energetic position of, e.g., an Au−S state.[74,75] Instead, we find a continuum of states in the "intragap" region (i.e., the energy range between HOPS and LUPS) that all have significant contributions on the metal and the docking group.[65]

Conceptually, the line-up of the frontier MOs with the metal E_F can also be understood on the basis of the schematic diagram shown in Figure 4. With the (saturated) molecular layer (Figure 4c) still isolated from the clean gold surface (Figure 4a), the initial level alignment is determined by the energy difference between IP_{left} [EA_{left}] and $\Phi_{Au(111)}$. Upon establishing contact, BD, to a first approximation, shifts the electrostatic potential in the spatial region of the molecular layer relative to E_F and, accordingly, also the molecular energy levels (Figure 4b). This leads to the final band alignment (Figure 4d), best described by the energy difference between the HOPS [LUPS] and E_F, ΔE_{HOPS} [ΔE_{LUPS}] (Table 2).

As a secondary effect, the bond formation between metal and molecule slightly perturbs the electronic structure of the molecules. To quantify the extent of this perturbation (E_{corr}^{HOMO} and E_{corr}^{LUMO}), we compare IP_{right} [EA_{right}] of the isolated molecular layer (Figure 2) with the energy difference between the HOPS [LUPS] and the vacuum level outside the SAM, IP_{SAM} [EA_{SAM}] (Figure 4d and Table 2). The values for E_{corr}^{HOMO} and E_{corr}^{LUMO} are typically $\leq$0.3 eV; in most cases, they decrease with increasing chain length as the local electronic perturbation around the metal−molecule bond contributes to a lesser extent to the overall electronic structure of the molecules. Significantly larger values are found only for the LUPS in the case of the isocyanide (−NC) docking group and the HOPS in the case of the −Pyr docking group. For the former, this can be attributed to the uncertainty in the determination of the energetic position of the LUPS (see Supporting Information). For the latter, a new state appears in the intragap region, mainly localized on the gold substrate and the N atoms (Figure 5); the appearance of this Au−N state can be held accountable for the large energy correction to the neighboring π-states (HOPS). Naturally, the *formation* of a new covalent bond between metal and molecules in the case of −NC and −Pyr leads to a stronger perturbation of the molecular electronic structure than the *substitution* of a bond in the case of −SH[65] and −SeH.

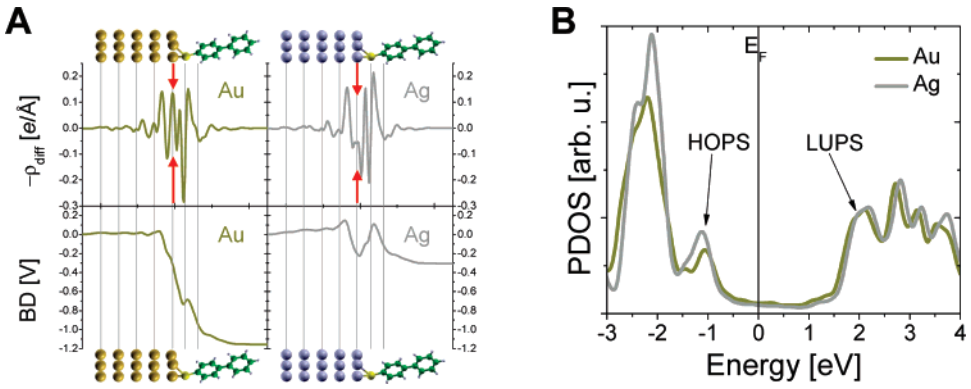

Figure 6. (a) Charge density rearrangement, ρ_{diff} (top), and resulting bond dipole, BD (bottom), occurring upon the formation of a SAM of 4-mercaptobiphenyl on Au(111) (left) and Ag(111) (right). The vertical lines indicate the positions of the metal, sulfur, and first carbon atoms and the arrows mark the region where the main difference between silver and gold occurs. (b) Density of states projected on to the molecular region (PDOS) of SAMs of 4-mercaptobiphenyl on Au(111) (yellow) and Ag(111) (gray). The vertical line marks the Fermi level, E_F; the energetic position of the HOPS and LUPS is also indicated.

To summarize, the alignment of the HOPS and LUPS relative to E_F can be expressed as:

$$\Delta E_{HOPS} = \Phi - IP_{left} + BD + E_{corr}^{HOMO} \quad (4.a)$$

$$\Delta E_{LUPS} = \Phi - EA_{left} + BD + E_{corr}^{LUMO} \quad (4.b)$$

with the values for the respective terms listed in Table 2. Note that different adsorption sites (see Supporting Information) may lead to a somewhat different chemical bond between docking group and metal, thus to slightly different BD and E_{corr} values and, consequently, to slightly different ΔE_{HOPS} and ΔE_{LUPS} values. However, careful testing and comparison with available literature data[38,53] indicates that these variations are inconsequential for the main conclusions drawn in the present work.

In general, the chain-length dependence of the molecular level energies is more pronounced for those levels that are farther away from E_F. Of particular interest is the case of the gold−pyridine system (Au|Pyr|*n*P|H with $n = 1...3$). Here, ΔE_{LUPS} is reduced noticeably upon increasing the length from 1P to 2P but remains constant upon further increasing the length from 2P to 3P: the Fermi level becomes *pinned* by the LUPS; it does not move *into* the delocalized π^*-states because this would lead to the electrostatically unfavorable situation of charging the molecule. Instead, the system responds by extending ρ_{diff}, and thus BD, farther into the molecular region (shaded region in Figure 3). Importantly, this observation indicates that, regardless of the relative energetic situation prior to adsorption, molecules of the type investigated here cannot be forced to line up their delocalized frontier π- or π^*-states with E_F. Rather, this situation is avoided by building up an alternating charge redistribution (a series of dipoles on the scale of bond-length distances) to readjust BD, thus keeping the molecules charge neutral as a whole. Similar observations have been made for the case of weakly bound (physisorbed) π-conjugated molecules[76] and polymers;[77,78] the energetic position of E_F within the gap of the organic could be tuned over a wide range but could not be forced *into* the HOPS or LUPS.

The mechanism of level alignment discussed above is in many ways reminiscent of the concepts developed for more conventional metal−semiconductor junctions, both organic[63,64] and inorganic.[60−62] However, by taking into account the full electronic structure at an atomistic level, we are able to derive here a more chemical insight into these concepts. In particular, our results underline the importance of the docking group for the interface energetics. First, it acts as a dipole layer between the metal and the π-conjugated core of the molecules and thus impacts the offset between the chemical potentials of the two subsystems (i.e., the driving force for charge equilibration). Second, the details of its chemical bonding to the metal and to the π-conjugated core determine the amount of interaction-induced broadening of each molecular level and, consequently, the number and spatial extent of (rapidly decaying[65,82]) states appearing within the molecular gap. Following concepts from classical semiconductor physics (like the charge-neutrality level[60−64]), electronic equilibration via charge flow from and into these states ultimately determines the nature of ρ_{diff} as well as the atomistic structure and magnitude of BD and thus the level alignment.

Impact of Substrate Metal. SAMs of organic molecules have been investigated on a variety of (noble) metal surfaces[5,6] in order to study the impact of the metal work function on single-molecule transport.[79,80] Here, we compare the most widely used metals, silver and gold, with an adsorbed SAM of the reference molecule, 4-mercaptobiphenyl, i.e., Au|S|2P|H and Ag|S|2P|H.

The data in Figure 6a shows that subtle differences in ρ_{diff} around the top layer of metal atoms add up to a substantially different absolute value for BD (Table 2) in the case of silver (−0.4 eV) as compared to gold (−1.2 eV). As a consequence of the different BD values (eq 3), $\Delta\Phi$ is smaller for silver than for gold covered with the same SAM (Table 1). Starting from a calculated work function $\Phi_{Au(111)} = 5.2$ eV for gold and $\Phi_{Ag(111)} = 4.5$ eV for silver (experimental values are 5.3 and 4.7 eV, respectively[81]), we find that, interestingly, the SAM-covered metal surfaces both end up with the same work function of $\Phi_{Au}^{mod} \approx \Phi_{Ag}^{mod} \approx 3.7$ eV. Similar observa-

tions have recently been made by Blom et al.[19] Most intriguingly, the different BD values for Ag and Au lead to the HOPS and LUPS lying at virtually the same energy with respect to E_F ($\Delta E_{HOPS} \approx -1$ eV and $\Delta E_{LUPS} \approx +2$ eV) for both metals (Figure 6b and Table 2). This indicates that, for the systems investigated here, the Fermi level is *pinned* between HOPS and LUPS and that changing the work function of the substrate by changing the metal from Ag to Au does *not* provide a handle for tuning the energetic position of the Fermi level in the molecular gap as would be the case in the Schottky−Mott limit. Again, the situation is reminiscent of junctions between metals and inorganic[60−62] as well as organic[63,64] semiconductors, where the Schottky barrier height (i.e., ΔE_{HOPS} and ΔE_{LUPS}) is often found to be independent of the metal work function.

Conclusions. For most applications of π-conjugated SAMs on metals, the two most relevant quantities are the relative alignment of the (broadened) molecular states relative to the metal Fermi level and the work function of the SAM-covered metal electrode. Our results illustrate that altering the electronic structure at the very SAM−metal interface by changing the docking chemistry significantly impacts both of these properties. As the SAM must be seen as a dipole layer, only the local ionization potential and electron affinity at the docking-group side of the SAM together with the interface dipole resulting from the bond formation are found to be relevant for the level alignment. This bond dipole together with the step in the vacuum potential across the SAM (resulting from the aligned molecular dipole moments) determines the work function modification. In all investigated systems, headgroup substitution on the far side of the molecule only change the SAM's local electrostatic potential on that side of the layer. Consequently, while hardly affecting the level alignment, these substitutions provide an additional, largely independent handle on the work function of the SAM-covered substrate.

Modifying the molecular conjugation length permits shifting the energy of the frontier molecular π-states without interfering with the bonding chemistry; we find that the Fermi level is pinned within the molecular gap for the strongly interacting thiol (selenol) and isocyanide linkers (albeit at different energies), while it gets pinned by the lowest unoccupied molecular π*-states in the case of pyridine. Changing the work function of the substrate by replacing gold with silver does not impact the level alignment and, interestingly, the two SAM-covered substrates are found to have virtually identical work functions.

Acknowledgment. We thank G. Kresse for his indispensable help with using the VASP code.[83−87] The work at Georgia Tech is partly supported by the National Science Foundation (through grant CHE-0342321, STC award DMR-0120967, and CRIF award CHE-0443564) and the Office of Naval Research. The financial support of the Austrian Science Foundation (FWF) through the Erwin−Schrödinger grant J2419-N02 and the Austrian Nano Initiative (project N-702-SENSPHYS) is gratefully acknowledged. This work has been conducted under the Marie-Curie OIF project INSANE (contract no. 021511).

Supporting Information Available: Methodology and extended discussion on isolated molecular layers, the adsorption pathway, charge transfer, and the perturbation of the molecular electronic structure upon binding to the metal. This material is available free of charge via the Internet at http://pubs.acs.org.

References

(1) Poirier, G. E. *Chem. Rev.* **1997**, *97*, 1117−1127.
(2) Schreiber, F. *J. Phys.: Condens. Matter* **2004**, *16*, R881−R900.
(3) Schreiber, F. *Prog. Surf. Sci.* **2000**, *65*, 151−256.
(4) Schwartz, D. K. *Annu. Rev. Phys. Chem.* **2001**, *52*, 107−137.
(5) Ulman, A. *Chem. Rev.* **1996**, *96*, 1533−1554.
(6) Love, J. C.; Estroff, L. A.; Kriebel, J. K.; Nuzzo, R. G.; Whitesides, G. M. *Chem. Rev.* **2005**, *105*, 1103−1169.
(7) Genzer, J.; Efimenko, K. *Science* **2000**, *290*, 2130−2133.
(8) Jennings, G. K.; Laibinis, P. E. *Colloids Surf., A* **1996**, *116*, 105−114.
(9) Eck, W.; Stadler, V.; Geyer, W.; Zharnikov, M.; Gölzhäuser, A.; Grunze, M. *Adv. Mater.* **2000**, *12*, 805−808.
(10) Felgenhauer, T.; Yan, C.; Geyer, W.; Rong, H. T.; Gölzhäuser, A.; Buck, M. *Appl. Phys. Lett.* **2001**, *79*, 3323−3325.
(11) Geyer, W.; Stadler, V.; Eck, W.; Zharnikov, M.; Gölzhäuser, A.; Grunze, M. *Appl. Phys. Lett.* **1999**, *75*, 2401−2403.
(12) Gooding, J. J.; Mearns, F.; Yang, W. R.; Liu, J. Q. *Electroanalysis* **2003**, *15*, 81−96.
(13) Halik, M.; Klauk, H.; Zschieschang, U.; Schmid, G.; Dehm, C.; Schütz, M.; Maisch, S.; Effenberger, F.; Brunnbauer, M.; Stellacci, F. *Nature* **2004**, *431*, 963−966.
(14) Kleineberg, U.; Brechling, A.; Sundermann, M.; Heinzmann, U. *Adv. Funct. Mater.* **2001**, *11*, 208−212.
(15) Kobayashi, S.; Nishikawa, T.; Takenobu, T.; Mori, S.; Shimoda, T.; Mitani, T.; Shimotani, H.; Yoshimoto, N.; Ogawa, S.; Iwasa, Y. *Nat. Mater.* **2004**, *3*, 317−322.
(16) Ishii, H.; Sugiyama, K.; Ito, E.; Seki, K. *Adv. Mater.* **1999**, *11*, 605−625.
(17) Kahn, A.; Koch, N.; Gao, W. Y. *J. Polym. Sci., Part B: Polym. Phys.* **2003**, *41*, 2529−2548.
(18) Campbell, I. H.; Rubin, S.; Zawodzinski, T. A.; Kress, J. D.; Martin, R. L.; Smith, D. L.; Barashkov, N. N.; Ferraris, J. P. *Phys. Rev. B* **1996**, *54*, 14321−14324.
(19) de Boer, B.; Hadipour, A.; Mandoc, M. M.; van Woudenbergh, T.; Blom, P. W. M. *Adv. Mater.* **2005**, *17*, 621−625.
(20) Alloway, D. M.; Hofmann, M.; Smith, D. L.; Gruhn, N. E.; Graham, A. L.; Colorado, R.; Wysocki, V. H.; Lee, T. R.; Lee, P. A.; Armstrong, N. R. *J. Phys. Chem. B* **2003**, *107*, 11690−11699.
(21) Campbell, I. H.; Kress, J. D.; Martin, R. L.; Smith, D. L.; Barashkov, N. N.; Ferraris, J. P. *Appl. Phys. Lett.* **1997**, *71*, 3528−3530.
(22) Ganzorig, C.; Kwak, K. J.; Yagi, K.; Fujihira, M. *Appl. Phys. Lett.* **2001**, *79*, 272−274.
(23) Hatton, R. A.; Day, S. R.; Chesters, M. A.; Willis, M. R. *Thin Solid Films* **2001**, *394*, 292−297.
(24) Yan, H.; Huang, Q. L.; Cui, J.; Veinot, J. G. C.; Kern, M. M.; Marks, T. J. *Adv. Mater.* **2003**, *15*, 835−838.
(25) Zehner, R. W.; Parsons, B. F.; Hsung, R. P.; Sita, L. R. *Langmuir* **1999**, *15*, 1121−1127.
(26) Zuppiroli, L.; Si-Ahmed, L.; Kamaras, K.; Nüesch, F.; Bussac, M. N.; Ades, D.; Siove, A.; Moons, E.; Grätzel, M. *Eur. J. Phys. B* **1999**, *11*, 505−512.
(27) Chen, J.; Reed, M. A.; Rawlett, A. M.; Tour, J. M. *Science* **1999**, *286*, 1550−1552.
(28) Bumm, L. A.; Arnold, J. J.; Cygan, M. T.; Dunbar, T. D.; Burgin, T. P.; Jones, L.; Allara, D. L.; Tour, J. M.; Weiss, P. S. *Science* **1996**, *271*, 1705−1707.
(29) Elbing, M.; Ochs, R.; Koentopp, M.; Fischer, M.; von Hänisch, C.; Weigend, F.; Evers, F.; Weber, H. B.; Mayor, M. *Proc. Natl. Acad. Sci.* **2005**, *102*, 8815−8820.
(30) Jiang, P.; Morales, G. M.; You, W.; Yu, L. P. *Angew. Chem., Int. Ed.* **2004**, *43*, 4471−4475.
(31) Kushmerick, J. G.; Holt, D. B.; Yang, J. C.; Naciri, J.; Moore, M. H.; Shashidhar, R. *Phys. Rev. Lett.* **2002**, *89*, 086802.
(32) Park, J.; Pasupathy, A. N.; Goldsmith, J. I.; Chang, C.; Yaish, Y.; Petta, J. R.; Rinkoski, M.; Sethna, J. P.; Abruna, H. D.; McEuen, P. L.; Ralph, D. C. *Nature* **2002**, *417*, 722−725.

(33) Reed, M. A.; Chen, J.; Rawlett, A. M.; Price, D. W.; Tour, J. M. *Appl. Phys. Lett.* **2001**, *78*, 3735−3737.
(34) Xue, Y. Q.; Datta, S.; Ratner, M. A. *J. Chem. Phys.* **2001**, *115*, 4292−4299.
(35) Vondrak, T.; Wang, H.; Winget, P.; Cramer, C. J.; Zhu, X. Y. *J. Am. Chem. Soc.* **2000**, *122*, 4700−4707.
(36) Xue, Y. Q.; Ratner, M. A. *Phys. Rev. B* **2003**, *68*, 115407.
(37) Patrone, L.; Palacin, S.; Charlier, J.; Armand, F.; Bourgoin, J. P.; Tang, H.; Gauthier, S. *Phys. Rev. Lett.* **2003**, *91*, 096802.
(38) Yaliraki, S. N.; Kemp, M.; Ratner, M. A. *J. Am. Chem. Soc.* **1999**, *121*, 3428−3434.
(39) Donhauser, Z. J.; Mantooth, B. A.; Kelly, K. F.; Bumm, L. A.; Monnell, J. D.; Stapleton, J. J.; Price, D. W.; Rawlett, A. M.; Allara, D. L.; Tour, J. M.; Weiss, P. S. *Science* **2001**, *292*, 2303−2307.
(40) Lewis, P. A.; Inman, C. E.; Maya, F.; Tour, J. M.; Hutchison, J. E.; Weiss, P. S. *J. Am. Chem. Soc.* **2005**, *127*, 17421−17426.
(41) Venkataraman, L.; Klare, J. E.; Tam, I. W.; Nuckolls, C.; Hybertsen, M. S.; Steigerwald, M. L. *Nano Lett.* **2006**, *6*, 458−462.
(42) Xu, B. Q.; Tao, N. J. J. *Science* **2003**, *301*, 1221−1223.
(43) Xu, B. Q.; Xiao, X. Y.; Tao, N. J. *J. Am. Chem. Soc.* **2003**, *125*, 16164−16165.
(44) Xu, B. Q. Q.; Li, X. L. L.; Xiao, X. Y. Y.; Sakaguchi, H.; Tao, N. J. J. *Nano Lett.* **2005**, *5*, 1491−1495.
(45) Yasuda, S.; Yoshida, S.; Sasaki, J.; Okutsu, Y.; Nakamura, T.; Taninaka, A.; Takeuchi, O.; Shigekawa, H. *J. Am. Chem. Soc.* **2006**, *128*, 7746−7747.
(46) Dholakia, G. R.; Fan, W.; Koehne, J.; Han, J.; Meyyappan, M. *Phys. Rev. B* **2004**, *69*, 153402.
(47) Selzer, Y.; Cai, L. T.; Cabassi, M. A.; Yao, Y. X.; Tour, J. M.; Mayer, T. S.; Allara, D. L. *Nano Lett.* **2005**, *5*, 61−65.
(48) Heimel, G.; Romaner, L.; Bredas, J. L.; Zojer, E. *Phys. Rev. Lett.* **2006**, *96*, 196806.
(49) Chen, J.; Calvet, L. C.; Reed, M. A.; Carr, D. W.; Grubisha, D. S.; Bennett, D. W. *Chem. Phys. Lett.* **1999**, *313*, 741−748.
(50) Dupraz, C. J. F.; Beierlein, U.; Kotthaus, J. P. *ChemPhysChem.* **2003**, *4*, 1247−1252.
(51) Hou, S. M.; Zhang, J. X.; Li, R.; Ning, J.; Han, R. S.; Shen, Z. Y.; Zhao, X. Y.; Xue, Z. Q.; Wu, Q. *Nanotechn.* **2005**, *16*, 239−244.
(52) Hu, Y. B.; Zhu, Y.; Gao, H. J.; Guo, H. *Phys. Rev. Lett.* **2005**, *95*, 156803.
(53) Ke, S. H.; Baranger, H. U.; Yang, W. T. *J. Am. Chem. Soc.* **2004**, *126*, 15897−15904.
(54) Kim, B.; Beebe, J. M.; Jun, Y.; Zhu, X.-Y.; Frisbie, C. D. *J. Am. Chem. Soc.* **2006**, *128*, 4970−4971.
(55) Patrone, L.; Palacin, S.; Bourgoin, J. P.; Lagoute, J.; Zambelli, T.; Gauthier, S. *Chem. Phys.* **2002**, *281*, 325−332.
(56) Perez-Jimenez, A. J. *J. Phys. Chem. B* **2005**, *109*, 10052−10060.
(57) Wu, X. J.; Li, Q. X.; Huang, J.; Yang, J. L. *J. Chem. Phys.* **2005**, *123*, 184712.
(58) Xue, Y. Q.; Ratner, M. A. *Phys. Rev. B* **2004**, *69*, 085403.
(59) Zangmeister, C. D.; Robey, S. W.; van Zee, R. D.; Kushmerick, J. G.; Naciri, J.; Yao, Y.; Tour, J. M.; Varughese, B.; Xu, B.; Reutt-Robey, J. E. *J. Phys. Chem. B* **2006**, *110*, 17138−17144.
(60) Bardeen, J. *Phys. Rev.* **1947**, *71*, 717−727.
(61) Tersoff, J. *Phys. Rev. Lett.* **1984**, *52*, 465−468.
(62) Tersoff, J. *Phys. Rev. B* **1985**, *32*, 6968−6971.
(63) Vásquez, H.; Flores, F.; Oszwaldowski, R.; Ortega, J.; Pérez, R.; Kahn, A. *Appl. Surf. Sci.* **2004**, *234*, 107−112.
(64) Vásquez, H.; Oszwaldowski, R.; Pou, P.; Ortega, J.; Pérez, R.; Flores, F.; Kahn, A. *Europhys. Lett.* **2004**, *65*, 802−808.
(65) Heimel, G.; Romaner, L.; Bredas, J. L.; Zojer, E. *Surf. Sci.* **2006**, *600*, 4548−4562.
(66) Chen, Y. C.; Cunningham, J. E.; Flynn, C. P. *Phys. Rev. B* **1984**, *30*, 7317−7319.
(67) Lang, N. D.; Kohn, W. *Phys. Rev. B* **1971**, *3*, 1215−1223.
(68) Ishi, S.; Viswanathan, B. *Thin Solid Films* **1991**, *201*, 373−402.
(69) Lang, N. D. *Phys. Rev. Lett.* **1981**, *46*, 842−845.
(70) Lang, N. D.; Norskov, J. K. *Phys. Rev. B* **1983**, *27*, 4612−4616.
(71) Iwamoto, M.; Mizutani, Y.; Sugimura, A. *Phys. Rev. B* **1996**, *54*, 8186−8190.
(72) Maschhoff, B. L.; Cowin, J. P. *J. Chem. Phys.* **1994**, *101*, 8138−8151.
(73) Kang, J. F.; Liao, S.; Jordan, R.; Ulman, A. *J. Am. Chem. Soc.* **1998**, *120*, 9662−9667.
(74) Zangmeister, C. D.; Robey, S. W.; van Zee, R. D.; Yao, Y.; Tour, J. M. *J. Phys. Chem. B* **2004**, *108*, 16187−16193.
(75) Zangmeister, C. D.; Robey, S. W.; van Zee, R. D.; Yao, Y. X.; Tour, J. M. *J. Am. Chem. Soc.* **2004**, *126*, 3420−3421.
(76) Braun, S.; Osikowicz, W.; Wang, Y.; Salaneck, W. R. *Org. Electron.* **2007**, *8*, 14−20.
(77) Crispin, A.; Crispin, X.; Fahlman, M.; Berggren, M.; Salaneck, W. R. *Appl. Phys. Lett.* **2006**, *89*, 213503.
(78) Tengstedt, C.; Osikowicz, W.; Salaneck, W. R.; Parker, I. D.; Hsu, C. H.; Fahlman, M. *Appl. Phys. Lett.* **2006**, *88*, 053502.
(79) Beebe, J. M.; Engelkes, V. B.; Miller, L. L.; Frisbie, C. D. *J. Am. Chem. Soc.* **2002**, *124*, 11268−11269.
(80) Engelkes, V. B.; Beebe, J. M.; Frisbie, C. D. *J. Am. Chem. Soc.* **2004**, *126*, 14287−14296.
(81) Michaelson, H. B. *J. Appl. Phys.* **1977**, *48*, 4729−4733.
(82) Langlais, V. J.; Schlittler, R. R.; Tang, H.; Gourdon, A.; Joachim, C.; Gimzewski, J. K. *Phys. Rev. Lett.* **1999**, *83*, 2809−2812.
(83) Kresse, G.; Furthmüller, J. *Comp. Mater. Sci.* **1996**, *6*, 15−50.
(84) Kresse, G.; Furthmüller, J. *Phys. Rev. B* **1996**, *54*, 11169−11186.
(85) Kresse, G.; Hafner, J. *Phys. Rev. B* **1993**, *47*, 558−561.
(86) Kresse, G.; Hafner, J. *Phys. Rev. B* **1994**, *49*, 14251−14269.
(87) Kresse, G.; Joubert, D. *Phys. Rev. B* **1999**, *59*, 1758−1775.

NL0629106